High-Efficiency Polymer-Based Direct Multi-Jet Impingement Cooling Solution for High-Power Devices

Tiwei Wei, *Student Member, IEEE*, Herman Oprins, *Member, IEEE*, Vladimir Cherman, *Member, IEEE*, Jun Qian, Ingrid De Wolf, *Senior Member, IEEE*, Eric Beyne, *Senior Member, IEEE*, and Martine Baelmans

***Abstract*—A high-efficiency three-dimensionally (3-D) shaped polymer multi-jet impingement cooler based on cost-efficient fabrication techniques is introduced for the cooling of high-power applications. State-of-the-art highly efficient multi-jet cooling solutions rely on expensive Si or ceramic fabrication techniques, while low-cost cooling solutions have been proposed for less performant single-jet impingement. In this paper, we present the concept, modeling, design, fabrication, experimental characterization, and benchmarking with literature data of a multi-jet impingement based liquid cooling solution, fabricated using low-cost polymer fabrication techniques, targeted to directly cool the backside of high-power devices. For the modeling study, unit cell model and full system level models are used to study the nozzle array scaling trends and thermal and fluidic jet-to-jet interactions. Furthermore, design guidelines for high-power electronics cooling are provided, including geometry selections, material selection, and fabrication techniques. Based on the design guidelines and cooling concept, this paper demonstrates a 3-D-shaped polymer impingement cooler with a 4 $\times$ 4 nozzle array, showing a very good thermal performance with low required pumping power. The multi-jet cooler can achieve heat transfer coefficients up to 6.25 $\times$ 10^4 W/m^2·K with a pump power as low as 0.3 W. The benchmarking study confirms furthermore that multi-jet cooling is more efficient than single-jet cooling and that direct cooling on the backside of the semiconductor device is more efficient than cooling the substrate or base plate.**

***Index Terms*—High power, jet impingement cooling, liquid cooling, low-cost fabrication, power electronics.**

Manuscript received July 2, 2018; revised September 11, 2018; accepted September 22, 2018. Date of publication September 30, 2018; date of current version May 2, 2019. This work was performed as part of the imec Industrial Affiliation Program on 3D System Integration and has been strongly supported by the imec partners and the imec Reliability, Electrical testing, Modeling and 3D technology teams. Recommended for publication by Associate Editor K. Ngo. *(Corresponding author: Tiwei Wei.)*

T. Wei was with the Department of Mechanical Engineering, Katholieke Universiteit Leuven, Leuven 3001, Belgium. He is now with imec, Leuven 3001, Belgium (e-mail: Tiwei.wei@imec.be).

H. Oprins, V. Cherman, and E. Beyne are with imec, Leuven 3001, Belgium (e-mail: oprins@imec.be; cherman@imec.be; beyne@imec.be).

J. Qian and M. Baelmans are with the Department of Mechanical Engineering, Katholieke Universiteit Leuven, Leuven 3001, Belgium (e-mail: jun.qian@kuleuven.be; martine.baelmans@kuleuven.be).

I. De Wolf is with the Department of Materials Engineering, Katholieke Universiteit Leuven, Leuven 3001, Belgium, and also with imec, Leuven 3001, Belgium (e-mail: dewolf@imec.be).

Color versions of one or more of the figures in this paper are available online at http://ieeexplore.ieee.org.

Digital Object Identifier 10.1109/TPEL.2018.2872904

I. Introduction

The recent trends in high-power electronics show an increase in device power density due to the reduction in device size, combined with rising demands on control, energy efficiency, and reliability [1]. For high-power insulated gate bipolar transistors (IGBTs) modules, the heat flux in the transistor packages approaches 300 W/cm^2 [2], while for wide bandgap transistor electronics like GaN for radar and telecommunication applications, the local power densities can be as high as 1 kW/cm^2 averaged over the chip [3]. To cope with the increasing heat flux challenge for future high-power devices on the order of 600–1000 W/cm^2 [4], conventional liquid cooling solutions such as (microchannel) cold plates are no longer sufficient, and a transition toward direct liquid cooling, which achieves higher cooling rates, will be required. The main drawbacks of the conventional cold plates are 1) the presence of the thermal interface material (TIM), which represents a major thermal resistance contribution and 2) the temperature gradient along the chip surface in the flow direction. A comparison of the cooling performance among cold plates, microchannel cooling, and jet impingement cooling is presented in the literature from an experimental [5] and numerical [6] perspective. The experimental study [5] shows that for a constant device junction temperature of 175 °C, the power dissipation capability of 60 W in the case of the cold plate can be increased to 99 and 167 W, respectively, for a microchannel cooler and a jet impingement cooler. The computational fluid dynamics (CFD) modeling study in [6] shows that jet impingement cooling designs with distributed outlets have the following advantages over microchannels cold plates and jet impingement coolers with common outlets: lower average chip temperature, improved temperature uniformity, and lower pressure drops in the cooler. Liquid jet impingement cooling can be applied on the power module baseplate, on the substrate, or even on the bare die. Bare die liquid jet impingement cooling is the most efficient cooling option where the liquid coolant is directly ejected from nozzles on the heat source backside resulting in a high cooling efficiency due to the absence of the TIM and the lateral temperature gradient. Moreover, it can be used as hotspot targeted cooling by delivering high localized heat transfer rates at the location of the hot spot(s), which can improve the temperature uniformity. Recently, a cost-efficient cooling solution for a single MOSFET semiconductor based on

0885-8993 © 2018 IEEE. Personal use is permitted, but republication/redistribution requires IEEE permission.
See http://www.ieee.org/publications_standards/publications/rights/index.html for more information.

Authorized licensed use limited to: Purdue University. Downloaded on January 16,2023 at 20:04:53 UTC from IEEE Xplore. Restrictions apply.

a single-jet direct impingement cooler was introduced [7]. This single chamber cooler with relatively larger nozzle diameter and simplified injection manifold can achieve heat transfer coefficients of 1.2×10^4 W/m^2·K for a pumping power of 0.9 W. Single-jet cooling is, however, limited to the efficient cooling of single hot spots since the obtained heat coefficient distribution is strongly nonuniform, where the cooling efficiency quickly decays from the stagnation point toward the wall jet region, which can generate significant thermal gradients. Liquid multi-jet array impingement cooling at the other hand provides the scalability of the high heat transfer coefficient area for areas from a few cm^2 to a few hundred cm^2, especially for multi-jet coolers with locally distributed outlets [8]. Furthermore, it is shown that cooling a hot spot array with a multi-jet cooler nozzle directed at hot spots is more efficient and achieves better temperature uniformity rather than cooling the complete surface area [9]. The main drawback of the multi-jet cooler is, however, the higher level of complexity to create the separate chambers for the fluid delivery and fluid extraction and the consequently added fabrication cost.

A. State-of-the-Art Impinging Jet Cooling

In the literature, a large variety of multi-jet impingement coolers fabricated with different materials and a large range of nozzle diameter values can be found. A selection of these multi-jet coolers has been summarized in Table I, which lists the cooler material, nozzle array geometry, and the achieved thermal performance. Fig. 1(a) shows the range of the nozzle diameters and the nozzle density for the considered impingement coolers, where the increase in nozzle density and the consequent reduction of the nozzle diameters result in an increasing complexity for the cooler fabrication. Multi-jet impingement coolers can achieve very high heat transfer coefficients. However, in the case of the small nozzle diameters, a high pressure and consequently high pumping power is required. The relation between the total cooling power of the impingement coolers and the required pumping power is shown in Fig. 1(b). In the figures, the chip area is used as the basis for the normalization of the heat flux, pumping power, and nozzle density.

Si fabrication techniques, including etching, allow the very precise fabrication of nozzles with small diameters. In the literature, several Si-fabrication-based impingement coolers with nozzle diameters of a few tens of μm have been presented for common returns, distributed returns, or combination of microchannels and impingement nozzles. In [10], Si-based single-jet and multi-jet impingement coolers with common returns are presented with diameters ranging from 40 to 76 μm, achieving a heat transfer coefficient of 0.9×10^4 W/m^2·K with the pump power of 6 mW. In [11], Brunschwiler *et al.* demonstrated that Si processing could be used to fabricate performant and complex microjet array impingement coolers with branched hierarchical parallel fluid delivery and return architectures with 50 000 inlet/outlet nozzles, allowing to increase the heat transfer coefficient to 8.7×10^4 W/m^2·K with 1.43W pump power. The main drawbacks of the Si-based coolers are the high pressure drop for the small diameter nozzles and the high fabrication cost. Other fabrication methods for nozzle diameters of a few hundred μm have been presented for ceramic and metal. Natarajan and Bezama [12] from IBM developed a microjet cooler with 1600 inlets and 1681 outlets using multilayer ceramic technology. Gould *et al.* [5] from Teledyne Scientific Company developed a compact jet impingement cooled metal heat exchanger with 48 200 μm diameter jets for a 600-V/50-A silicon carbide (SiC) power module used for bidirectional power conversion between a 28-V battery and a 300-V dc bus. Acikalin and Schroeder [13] from Intel Labs paper developed a stainless steel direct liquid contact microchannel cold plate for bare die packages. Liu *et al*. [14] demonstrated a metal-based bottom-side microjet array cooling heatsink for the thermal management for both the active radar systems and high-power density LEDs, in particular for LED array. International Mezzo Technologies [15] demonstrated a microjet cooler with honeycomb structure, which contains microjets with 300 μm diameter. A single-jet metal cooler [7] with an inlet diameter ranging from 0.6 to 1.6 mm was demonstrated on a bare MOSFET semiconductor device. Low-cost fabrication methods, including injection molding [16] and three-dimensional (3-D) printing [17], have been introduced for much larger nozzle diameters (mm range) with larger cooler dimensions. Whelan *et al.* [17] developed a miniature 3-D printed jet array waterblock using 49 individual 1 mm jets. Baumann *et al*. [16] demonstrated a module-level injection molded impingement cooler for the cooling of power electronic modules in hybrid electrical vehicle traction applications. These dimensions and processes are, however, not compatible with the chip packaging process flow.

The thermal performance of the cooling solution can be further improved by modifying the contact surface of the semiconductor device on which the liquid coolant is impinged. Ndao *et al.* [18] experimentally investigated that the heat transfer can be as high as 3.03 or about 200% increase by enhancing the target surface with a finned surface. This phenomenon can be exploited to develop "hybrid" microheat sinks, which contain impingement cooling channels as well as an array of fins created in the semiconductor device to achieve very high cooling rates. Han *et al*. [19] from IME proposed a package-level hotspot cooling solution for GaN transistors using a Si microjet/microchannel hybrid heat sink, which can enable a high spatially average heat transfer coefficient of 18.9×10^4 W/m^2·K with the low pumping power of 0.17 W. Robinson *et al*. [20] developed a micro-heat sink designed with microchannels and an array of fins with integrated microjets using a metallic additive manufacturing process resulting in a heat transfer coefficient of 30×10^4 W/m^2·K. These hybrid approaches are, however, a very disruptive cooling technology, requiring the etching of structures inside the device to be cooled.

The overview of the literature study, summarized in Table I, shows a large variety for the number of nozzles and the nozzle diameters for the impingement coolers for power electronic devices. However, a systematic study to determine the optimal nozzle array geometry in order to optimize the thermal as well as the hydraulic performance is missing. In this paper, we present a modeling study to investigate the thermal performance scaling trend of the number of nozzles and the nozzle diameter for multi-jet impingement coolers, to derive a guideline for the

Authorized licensed use limited to: Purdue University. Downloaded on January 16,2023 at 20:04:53 UTC from IEEE Xplore. Restrictions apply.

TABLE I
REVIEW OF STATE-OF-THE-ART COOLING SOLUTIONS

Material	Authors	Application	Coolant/ Phase	Number of jets	Nozzle diameter	Chip area	Power/Heat flux	Flowrate/Pressure drop/Pump power	Thermal Performance
Si	2004,[10], E.N. Wang	TTV	Water/Tin=23° C	4	76 μm	1 cm^2	4W	FL=8 mL/min $\Delta p = 47.57$ KPa	h_{max}=4.4 W/(cm^2K)
Si	2010, [27] E.A.Browne	MEMS fabricated device-	Single phase Water Tin=23°C	17	112μm	1mm^2	930 W/cm^2	$\Delta p = 348$ KPa	h_{avg}=31.8 W/(cm^2K)
Si	2006, [11], T.Brunschwiler	CPU-Si die	Water/ single-phase	50000	31-103 μm	4 cm^2	370 W/cm^2	FL=2.5 L/min Δp =35KPa Q_{Pump}=1.46 W	R_{avg}= 0.17 Kcm^2/W h_{av}=8.7 W/(cm^2K) uniformity < 0.5°C
Si* Hybdrid	2007, [28] E. G. Colgan	Bare die	Water@22°C	Channel pitch: 60-100 μm 450 μm thick channel		4 cm^2	400 W/cm^2	FL=1.25 L/min Δp =34.5 KPa Q_{Pump}=0.72 W	R_{avg}=0.026 K/W
Si* Hybrid	2015, [19] Yong Han	GaN device with diamond heat spreader	Single Phase Tin=25°C	21×11	100μm	0.49cm^2	110W; 260 W/cm^2	Q_{Pump}=0.05W	R_{avg}= 0.09 Kcm^2/W
Plastic	2012, [17] B.P. Whelan	Heater block mimic CPU	Water Tin=15°C	49	1mm	8.24 cm^2	200W	FL=10 L/min Δp =37.5 KPa Q_{Pump}=6.25 W	R_{avg} =0.076 K/W
Plastic	2015, [29], C.S. Sharma	Bare TTV die	Water Single phase Tin=20°C	Slot nozzle width		6.26 cm^2	285W; 150W/cm^2	FL=1.2 L/min Δp =33 KPa Q_{Pump}=0.66 W	R_{avg}= 0.2 Kcm^2/W
Plastic	2016, [2], A. S. Bahman	IGBT module	Glycol 50-water 50; Tin=20°C	40 channels	2.5-3mm wide Channel	—	IGBT:50W Diode: 25W	$\Delta p = 26$ KPa FL=5 L/min Q_{Pump}=1.27 W	R_{avg}=0.2 K/W
Plastic	2006,[9], Klaus Olesen	IGBT module	Ethylene-glycol/water 50%/50%	—	—	7.47cm^2	—	Δp =0.19 bar FL=12 L/min Q_{Pump}=3.8 W	R_{avg}= 0.97 Kcm^2/W
Ceramic	2007, [12] G. Natarajan	CPU-Si die	liquid single-phase Tin=20°C	1600	126 μm	1.8cm^2	290W/cm^2	FL=1.2 L/min Δp =53 kPa Q_{Pump}=1.06 W	h_{avg}=5.2 W/(cm^2K) R_{avg}= 0.053 K/W
Metal	2015, [5], Kyle Gould	SiC power module base plate	Water–ethylene glycol/ Tin=100 °C	48	200 μm	0.64 cm^2 (16 legs)	151W	FL=195 ml/min Δp =34.47 kPa Q_{Pump}=0.11 W	T_j = 175 °C R_{avg}=0.28 Kcm^2/W
Metal	2007, [15] Overholt MR	Electrical device	Water	11×11	200-300μm	1cm^2	1.5 kW/cm^2		h_{avg}=50 W/(cm^2K) R_{avg}=0.02 K/W
Metal	2014, [13] Tolga Acikalin	VLSI Si device	Liquid/ Single phase Tin=22°C	240	300μm	1.18cm^2 Cooler	40W	FL=1.18 L/min Δp =41.4kPa Q_{Pump}=0.81 W	R_{avg}=0.24 Kcm^2/W
Metal	2008, [30], M. K. Sung	TTV	HFE 7100 - 40°C to 20°C	5x14	390μm	2 cm^2	16.1-304.9W/cm^2	FL=6.82 to 45.5 mL/min	
Metal	2012, [26], Skuriat, Robert	Si diode with AlN substrate	40 °C water	36	0.5mm	12.7mm^2	150W 93 W/cm^2	Q_{Pump}=6W	R_{avg}=0.2 K/W
Metal	2017, [23], J. Jorg	IGBT-module	22.5 °C water	1	0.6 mm	25mm×35mm	125W	FL=300ml/min Q_{Pump}=0.1W	h_{avg}=0.5 W/(cm^2K)
Metal	2018, [7], J. Jorg	MOSFET Device	22.5 °C water	1	0.6 mm	0.64 cm^2	51W	FL=30 ml/min Q_{Pump}=3mW	h_{avg}=1.2 W/(cm^2K)
Metal* Hybrid	2018, [20], A.J. Robinson	Heater block	20°C water	100	30μm	3.1×4.2 mm^2	1000 W/cm^2	FL=0.5 L/min Δp =160 kPa Q_{Pump}=1.3W	h_{avg}=30 W/(cm^2K) R_{avg}=0.03 Kcm^2/W

cooler design and to predict the cooler's thermal and hydraulic performance for an arbitrary chip size.

B. Polymer-Based Multi-Jet Cooling Concept

The presented literature study shows that multi-jet impingement coolers can achieve very high cooling rates, but their major drawback is the complex and expensive fabrication. In this paper, we present a cost-efficient high-efficiency multi-jet impingement cooling solution, fabricated using low-cost polymer fabrication techniques, targeted to directly cool the backside of high-power semiconductor devices. The purpose of this work is to demonstrate the feasibility of an integrated polymer impingement cooler and to benchmark its thermal performance

Authorized licensed use limited to: Purdue University. Downloaded on January 16,2023 at 20:04:53 UTC from IEEE Xplore. Restrictions apply.

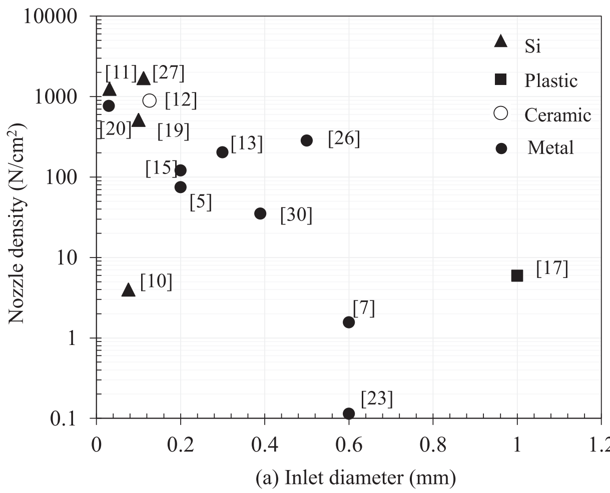

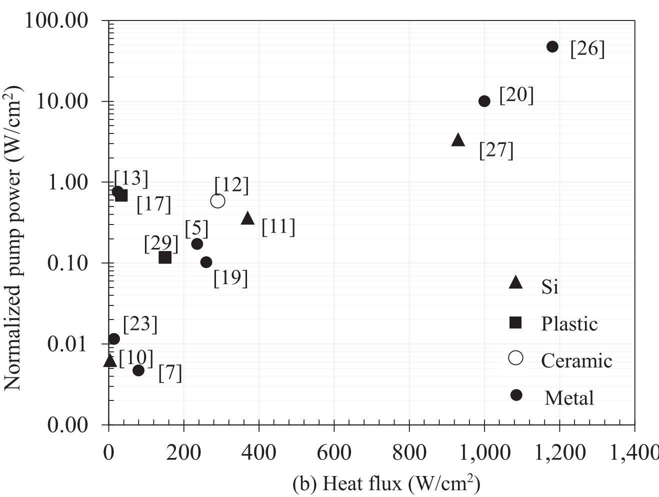

Fig. 1. Graphical representation of the geometrical, thermal, and hydraulic specifications of the literature survey in Table I. (a) Trend of the nozzle density on the chip area as a function of the nozzle diameter. (b) Trend of the normalized required pump power in the cooler as a function of the dissipated heat flux in the chip. All quantities are normalized with respect to the chip area.

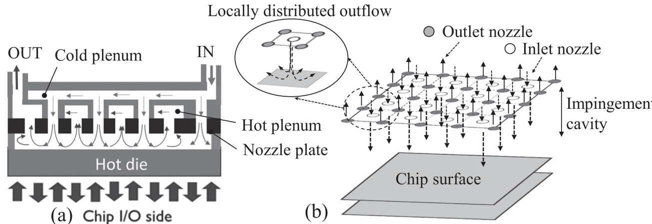

Fig. 2. Concept of the 3-D-shaped polymer cooler. (a) Cross section of the multi-jet cooler internal structure. (b) Side view of the distributed inlets and outlets in the nozzle plate.

with literature data for impingement coolers with various materials. The schematic of the model for impingement jet cooling with distributed inlet and outlet channels for the delivery and removal of the coolant is shown in Fig. 2. As shown in Fig. 2(a), the inlet flow first goes through the inlet plenum and distributes jets flow for individual inlet nozzles. After that, the fluid ejects through the inlet nozzles and impinges on the heated chip surface shown in Fig. 2(b). After striking on the chip surface, the fluid returns to the outlet plenum through the effusion nozzles. In order to evaluate the thermal performance, the fabricated 3-D-shaped polymer cooler is assembled to our 8×8 mm^2 thermal test chip, referred to as Packaging Test Chip Version Q (PTCQ) [21], with integrated heaters and temperature sensors. This thermal test chip is used to mimic the power electronic device.

The remainder of the paper is structured as follows. Section II describes the thermal and hydraulic modeling study of the impingement cooler. First, we present a unit cell based analysis to investigate the scaling trend with the number of nozzles and the nozzle diameter for multi-jet impingement coolers, to derive a guideline for the cooler design and to predict the cooler performance. Next, a full cooler level model is presented to study the system-level thermal and hydraulic effects. In Section III, results of the modeling study are applied to design the polymer cooler. Furthermore, the fabrication of the cooler is discussed. Section IV presents the experimental thermal characterization of the fabricated polymer cooler and the benchmarking of the cooler performance with respect to the coolers described in the literature study. Section V concludes the study.

II. Thermal and Hydraulic Modeling of the Impingement Cooler

The overview of impingement coolers in Table I shows a very large variety for the nozzle diameter (from tens of μm to tens of mm), for the number of nozzles (from single jet to more than 50 000), and for the materials used for the cooler fabrication. However, no thorough analysis of design considerations with regard to the impact of the nozzle geometry parameters, nozzle density, or the thermal impact of the cooler material is available. In this work, we present a modeling study to investigate the impact of the nozzle array geometry and the scaling of the number of nozzles for an $N \times N$ multi-jet impingement cooler with distributed returns, as shown in Fig. 1. Conjugate heat transfer fluid dynamics simulations (CHT-CFD) have been performed to assess the thermal and fluidic behavior of an impingement cooler with an $N \times N$ nozzle array considering water as a coolant. In the first step, a unit cell model, representing the nozzle array, is used to assess the optimal number of nozzles, nozzle pitch, and nozzle diameter for a large range of nozzle diameters and flow rates. In the next step, a full cooler level model is used to investigate the interaction between the different nozzles, the impact of the plenum design on the flow uniformity, and the impact of the cooler material.

The conjugate heat transfer models consider conduction and convection in the liquid domain of the model and conduction in the solid domain. This solid domain includes the silicon die with 0.2 mm thickness. A transition shear stress transport (SST) model is used for the CFD simulations, since this type of turbulence model offers a good compromise between accuracy and computational time for jet impingement modeling [22] and allows to cover the large range of Re numbers from laminar flow, over transitional flow to turbulent flow that is encountered in a practical cooling design. In this study, flow rates from 50

Authorized licensed use limited to: Purdue University. Downloaded on January 16,2023 at 20:04:53 UTC from IEEE Xplore. Restrictions apply.

ml/min up to 1000 ml/min have been considered. This corresponds to a range from 10 to 3500 for the Re_d number based on the nozzle diameter, while the reported laminar to turbulence transition range for liquid jet impingement is between 1000 and 3000 [22]. Based on this range of considered Re numbers from laminar to low Re turbulent flow, a Reynolds-averaged Navier–Stokes (RANS)-based transition SST model has been chosen, using "SIMPLE" algorithm as the solution method and the QUICK scheme for the numerical discretization. The convergence criteria were set at 10^{-5} for continuity, 10^{-6} for energy, and 10^{-6} for k, w, and momentum (x, y, and z velocities), respectively. Prism element cells are used for the meshing of the boundary layers with a minimal meshing size of 0.002 mm. The latter is calculated from the $y^+ < 1$ constraint for the turbulence model near boundaries [22]. The number of boundary layer grid cells in the normal direction to solid walls is set to 15. Tetrahedral element cells are used for the computation bodies with a complex internal structure. The number of elements for the unit cell model is around 0.6 million, while the full model is around 8.5 million based on the meshing sensitivity study. For the unit cell model and the full cooler level model, the grid sensitivity analysis using the Richardson extrapolation predicts a discretization error for the stagnation temperature of 0.2% and 0.3%, respectively. The power dissipation in the device is represented as a heat flux boundary condition on the Si. The flow conditions are applied as a velocity or pressure condition at the inlet and a pressure outlet boundary condition for the outlet. The results of interest from the simulation are the temperature distribution in the electronic device and the liquid coolant as well as the pressure drop required to pump the coolant through the cooler for the considered flow rate m or nozzle velocity V_{in}, which are related as follows for the $N \times N$ jet array:

$$\dot{V} = N^2 V_{\text{in}} A.$$

The required pumping power W_p can be expressed as

$$W_p = \dot{V} \Delta p$$

where the pressure drop Δp is defined as the difference between the inlet and the outlet static pressure. The thermal performance is expressed in terms of the thermal resistance R_{th}

$$R_{\text{th}} = (T_{\text{ch,avg}} - T_{\text{in}}) / P$$

where $T_{\text{ch, avg}}$ is the average chip temperature, T_{in} is the coolant inlet temperature, and P is the chip power. In order to optimize the performance of the cooler, a trade-off needs to be made between the improvement of the thermal resistance and the required pumping power to achieve this.

A. Unit Cell Modeling Study

Fig. 3(a) shows the top view of the nozzle plate of the impingement cooler for an $N \times N$ array where each inlet is surrounded by four outlets. This symmetrical nozzle array can be approximated by a unit cell of a single jet [see Fig. 3(b)], this ignoring effects from the side walls of the device. Due to the symmetry of the structure, this unit cell can be further reduced to a 1/8 model allowing a drastic reduction of the computation time for the design of experiments (DOE), considering the following five design parameters: nozzle number N, inlet diameter d_i, outlet diameter d_o, nozzle plate thickness t, and cavity height H. In addition, the simulations are performed for a range of flow conditions expressed in terms of flow rate, pressure drop, or pumping power, considering a uniform velocity profile at the inlet. In this study, the $N \times N$ jet array is matched to the 8×8 mm^2 chip size of the test vehicle. Table II shows the cooling density of the different unit cell sizes on the test chip. Moreover, the fabrication techniques linked with different cooling cell sizes are also illustrated in this table. $N \leq 16$ is in the range of the capability of polymer fabrication techniques, while higher nozzle numbers and smaller diameters would require more expensive Si fabrication techniques. For the DOE study of the unit cell modeling, the nozzles number will cover from a single jet to 32×32.

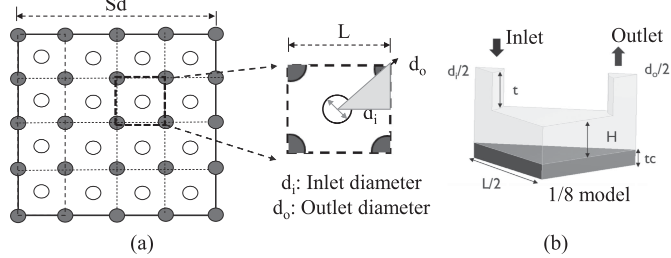

Fig. 3. Unit cell modeling approach. (a) Indication of cooler geometrical parameters and unit cell. (b) Coupled flow and thermal simulation result from a 1/8 detailed model, simplified from the unit cell.

TABLE II
SCALING OF THE NOZZLE GEOMETRY OF THE MULTI-JET COOLER FOR TWO NOZZLE DIAMETER TO UNIT CELL SIZE RATIOS AND THE LINK WITH FEASIBLE MANUFACTURING OPTIONS

N×N	Cooling density Cells per cm^2	Cooling cell size on PTCQ	Nozzle diameter ratio 1 (di/L=0.3)	Nozzle diameter ratio 2 (di/L=0.4)	Fabrication techniques
Single jet	1.56 / cm^2	8 × 8 mm^2	2.4 mm	3.2 mm	Mechanical machining process
2×2	6.25 / cm^2	4 × 4 mm^2	1.2 mm	1.6 mm	
3×3	14 / cm^2	2.67 × 2.67 mm^2	0.8 mm	1.07 mm	
4×4	25 / cm^2	2 × 2 mm^2	0.6 mm	0.8 mm	
6×6	56.25 / cm^2	1.33 × 1.33mm^2	0.4 mm	0.532 mm	Injection molding /3D Printing (**low cost**)
8×8	100 / cm^2	1 × 1 mm^2	0.3 mm	0.4 mm	
10×10	156.25 / cm^2	800 × 800 μm^2	0.24 mm	0.32 mm	
12×12	225 / cm^2	667 × 667 μm^2	0.2 mm	0.27 mm	
16×16	400 / cm^2	500 × 500 μm^2	0.15 mm	0.2 mm	
32× 32	1600 / cm^2	250 × 250 μm^2	0.075 mm	0.1 mm	Silicon processing (**expensive**)
64× 64	6400 / cm^2	125 × 125 μm^2	0.038 mm	0.05 mm	

Note: PTCQ (Packaging Test Chip Version Q) is defined as a dedicated thermal test chip, which is used to study the temperature response of impingement jet cooling.

Fig. 4 shows the temperature difference distribution over the chip surface to a fluid inlet for different numbers of nozzles in the array for a constant pressure drop across the nozzle plate. The comparison between the temperature distribution from the full cooler model and the reconstructed mirrored profile from the unit cell shows a good agreement between the unit cell and the full model, except for the small edge effects that are observed in the full model near the chip edges. The unit cell

Authorized licensed use limited to: Purdue University. Downloaded on January 16,2023 at 20:04:53 UTC from IEEE Xplore. Restrictions apply.

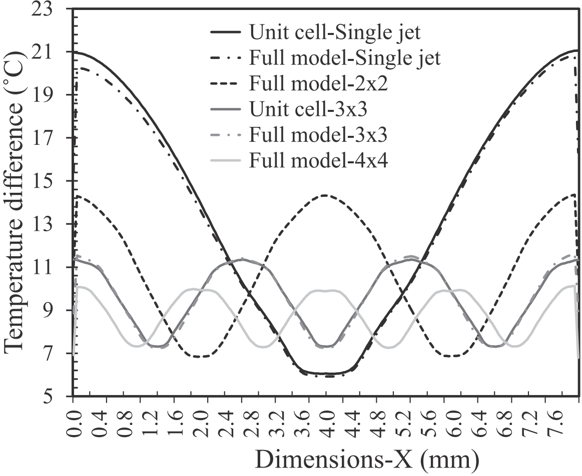

Fig. 4. Temperature difference (surface to fluid inlet) profile for N scaling ($di/L = 0.1$).

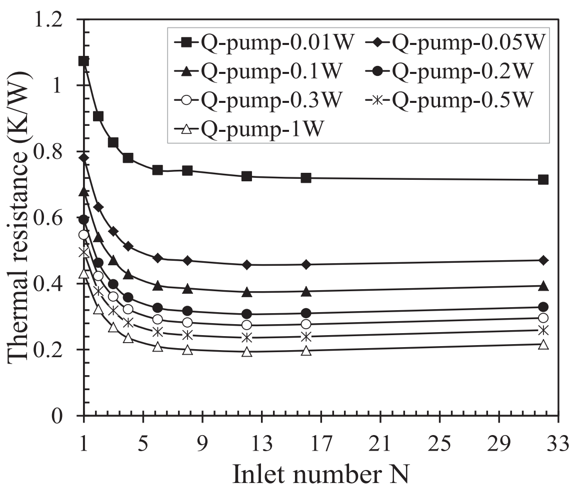

Fig. 6. Evolution of thermal resistance as a function of number of nozzles for constant pump power.

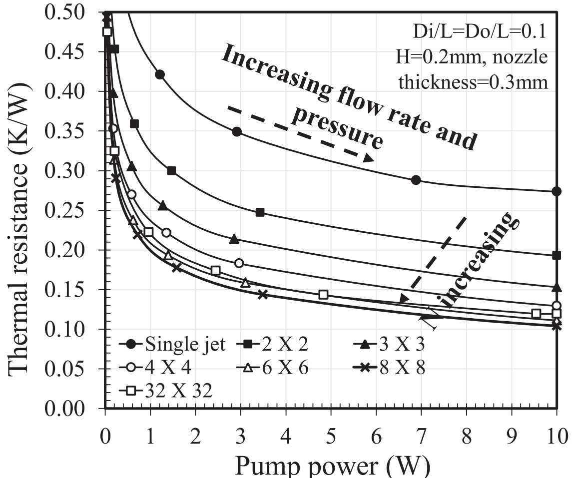

Fig. 5. Thermal resistance versus pump power tradeoff chart of the cooler thermal performance for increasing number of inlet nozzles N ($di/L = do/L = 0.1$) and fixed cavity height.

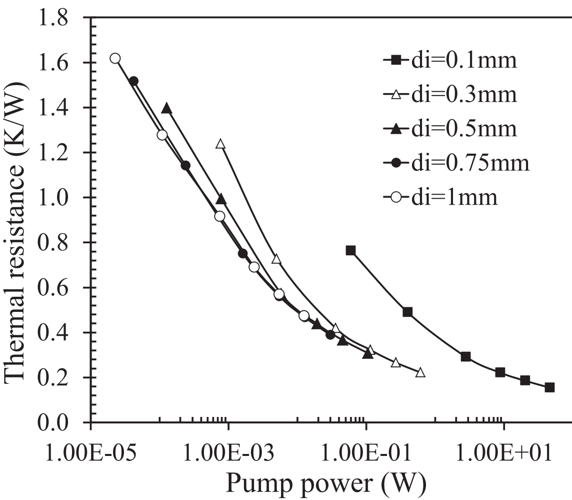

Fig. 7. Impact of nozzle diameter in a 4×4 array cooler (chip power: 100 W in 8×8 mm^2; inlet temperature: 10 °C; cavity height: 200 μm).

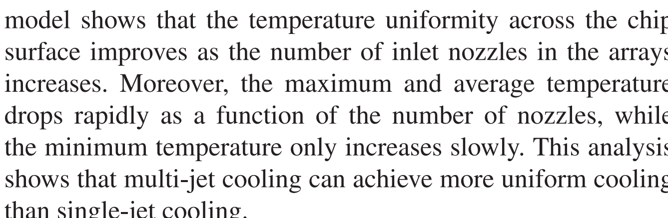

model shows that the temperature uniformity across the chip surface improves as the number of inlet nozzles in the arrays increases. Moreover, the maximum and average temperature drops rapidly as a function of the number of nozzles, while the minimum temperature only increases slowly. This analysis shows that multi-jet cooling can achieve more uniform cooling than single-jet cooling.

The thermal resistance can be further reduced by increasing the flow rate, however at the expense of the required pump power. This trade-off can be shown in a thermal resistance versus pumping power chart in which each cooler design is represented by a curve for a range of flow rates. The closer the curve to the origin, the better the thermal performance and the less the required pumping power of the cooler. In Fig. 5, this relation is shown for different cooler unit cell sizes with a fixed nozzle diameter to unit cell size ratio di/L and for a fixed cavity height of 200 μm. In this way, the scaling of the number of nozzles on the 8×8 mm^2 chip size is studied for a fixed overall nozzle area.

By using a high number of small diameter nozzles, one can achieve better thermal performance compared to the single-jet case. However, it requires a very high pressure and consequent pumping power, resulting in a saturation of the thermal performance increment beyond $N = 8$ on the 8×8 mm^2 chip size (1 mm^2 cooling unit cell). This trend can be clearly observed in Fig. 6 that shows the evolution of the thermal resistance as a function of the number of nozzles for several constant values of the pumping power. It should be noted that the analysis shown in Fig. 6 is based on the unit cell model in order to allow an extensive sensitivity analysis, and that consequently the plenum pressure drop and its impact on the scaling has not been included in this analysis. The impact of the nozzle diameter on the thermal and hydraulic performance is illustrated for a 4×4 nozzle array (2×2 mm^2 unit cell). The trade-off between thermal resistance and pumping power in Fig. 7 shows a better performance for larger nozzle diameters; however, in the range of the relevant pumping power of 0.1 W, the improvement saturates beyond $di/L = 0.3$.

Authorized licensed use limited to: Purdue University. Downloaded on January 16,2023 at 20:04:53 UTC from IEEE Xplore. Restrictions apply.

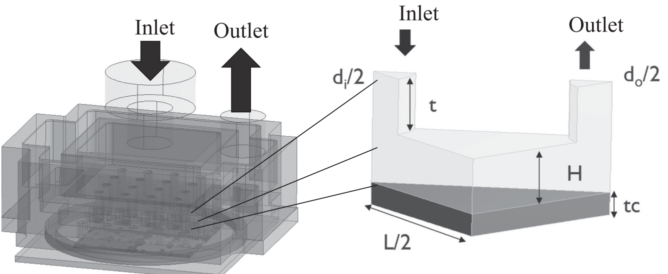

Fig. 8. Full cooler system level model.

The impact of the other parameters, the nozzle plate thickness, and the cavity height is less significant. For increasing nozzle plate thickness, the thermal resistance reduces slightly since the flow is more developed for longer nozzle lengths, resulting in higher peak velocities in the nozzle center. However, increasing the nozzle plate thickness from 500 μm to 1 mm only results in a reduction of the thermal resistance of 2% in the 4 × 4 jet array test case, while the pressure drop increases for the longer nozzle length. For this 4 × 4 array test case, the thermal performance is almost constant with respect to the cavity height in the range of 200–400 μm. Beyond 400 μm, there is a slight but steady deterioration of the thermal performance as the cavity height increases. For cavities below 200 μm, a sharp increase in the heat transfer can be observed; however, this happens at the expense of an even higher increase in the pressure drop, limiting the optimal range for the cavity. Therefore, this region is the pressure drop in relative quantity increasing more than the relative change in the heat transfer. Besides thermal and hydraulic aspect, reliability aspects and the structural strength also need to be considered. These aspects will impose additional constraints on the design parameters.

B. System-Level Modeling

The unit cell model assumes an identical behavior for each cooling cell in the jet array; however, in the cooler, there are differences in the flow rate and chip temperature between central nozzles and corner nozzles. In order to study the extent of this nonuniformity of the flow in the nozzle and nonuniformity of the chip temperature, a CFD model of the complete cooler is used. Fig. 8 shows the full model, including the cooler, coolant, chip, and package for the 4 × 4 array test case. This model allows to simulate the flow distribution in the nozzles, the interaction between different nozzles, and the impact of the plenum design and cooler material. Moreover, the complex flow phenomena can be visualized through the flow streamlines. Fig. 9(a) and (b) shows a contour plot of the flow velocity and the streamlines of the coolant in a diagonal cross-section of the cooler, respectively. The streamline plot shows that the jet-to-jet interaction of the neighboring nozzles is negligible since the crossflow effects are eliminated by using locally distributed outlets. This advantage shows the potential for hot spots targeted cooling without interfering other jet flows. The contour plot in Fig. 9(a) shows that for the considered inlet plenum height of 2.5 mm, a higher flow rate is observed in the central nozzles compared to the corner nozzles. Moreover, the thermal and hydraulic performance of

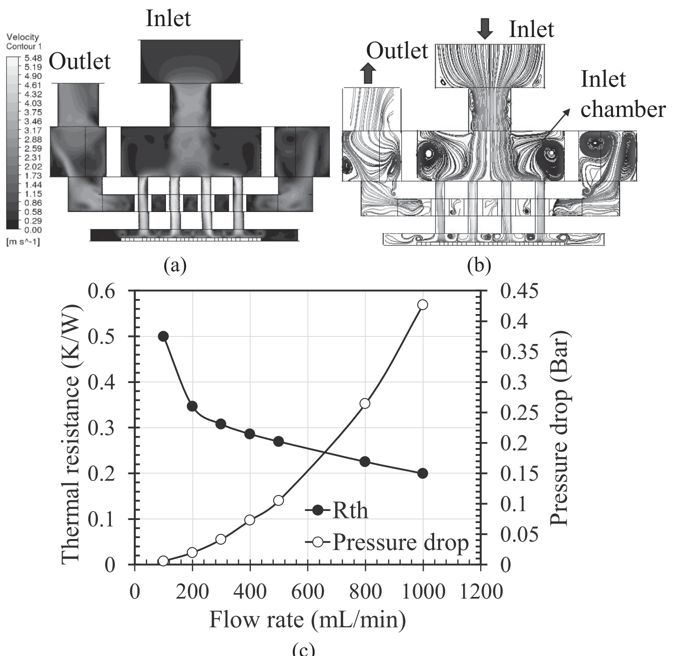

Fig. 9. Full system level model modeling results. (a) and (b) Velocity field and flow streamline visualization inside the full cooler. (c) Evolutions of pressure drop and thermal resistance as a function of flow rate.

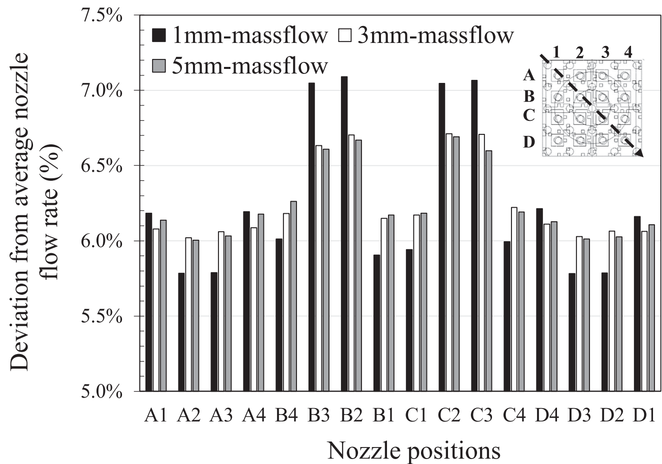

Fig. 10. Impact of the plenum level thickness on the flow distribution in the 4 × 4 array of inlet nozzles.

the full cooler model with 0.5 mm nozzle diameters is shown in Fig. 9(c). The modeling results show the trade-off between the thermal resistance and pressure drop under different flow rates.

The impact of the inlet plenum thickness on the flow distribution in the nozzles of the 4 × 4 array cooler is shown in Fig. 10 for three thickness values. A thin plenum with 1 mm height generates a significant flow maldistribution of more than 25% with higher velocity concentrating in the nozzles in the center of the cooler. This indicates that it is important to balance the inlet diameter and plenum height when designing the impingement cooler. For the thicker inlet plenum with 5 mm thickness, the flow distribution is much more uniform. However, the use of a thicker plenum increases the total cooler thickness.

In order to study the impact of the cooler material on the chip temperature for different flow rates, a dedicated simplified

Authorized licensed use limited to: Purdue University. Downloaded on January 16,2023 at 20:04:53 UTC from IEEE Xplore. Restrictions apply.

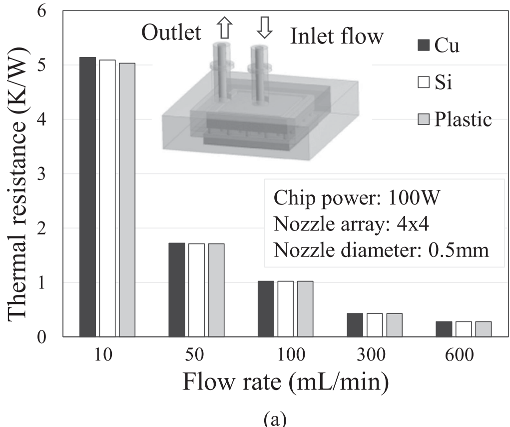

(a)

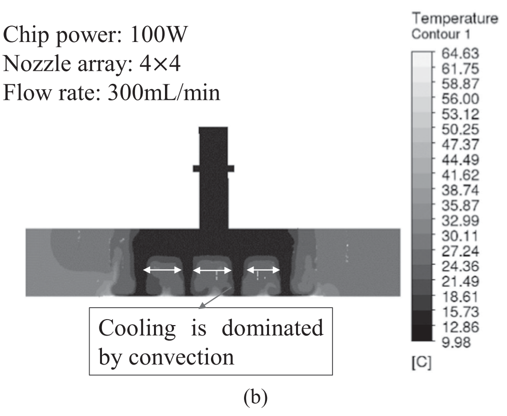

(b)

Fig. 11. Contour plots of the full cooler CFD models showing (a) the impact of the thermal conductivity of the cooler materials for different flow rates and (b) temperature distributions (chip power 100 W).

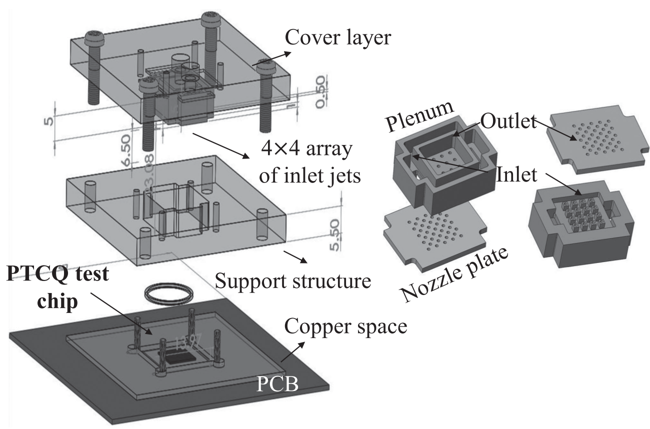

Fig. 12. CAD design structure of the 4 × 4 array demonstrator of the impingement cooler and integration on the test chip and PCB.

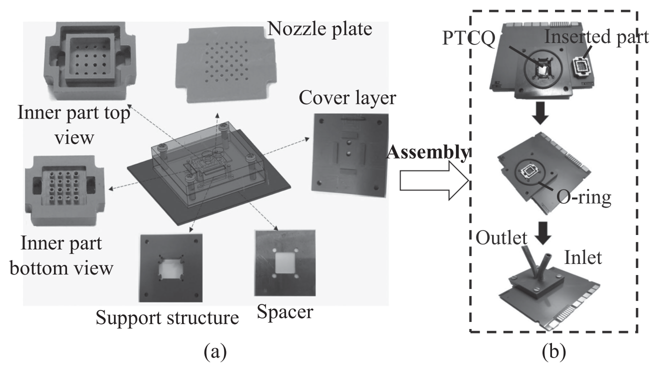

(a) (b)

Fig. 13. (a) Different fabricated parts of the 4 × 4 array demonstrator of the impingement cooler. (b) Final assembly of the 4 × 4 array demonstrator of the impingement cooler and integration on the test chip and PCB.

full model shown in Fig. 11 is simulated under a large range of flow rates from 50 to 600 ml/min. The considered materials are Cu (401 W/m·K), Si (1484 W/m·K), and polymer (0.2 W/m·K). The cooling performance comparison with the three different cooler materials is shown in Fig. 11(a). The simulations show that the impact of the cooler thermal conductivity on the chip temperature distribution is negligible over a wide range of flow rates and chip power values, as shown in Fig. 11(b). The modeling results show that a polymer cooler has even a slightly better performance than a Cu cooler, as it prevents the incoming coolant from heating up by the exiting coolant flow. This offers opportunities for the use of polymer-based cost-efficient fabrication techniques.

III. Design and Fabrication of the Micromachined Cooler

Based on the thermal and hydraulic modeling results for the number of unit cells, inlet diameter, and impact of material conductivity, and on the fabrication capabilities, a simplified board-level polymer demonstrator cooler has been designed to be manufactured in polyvinyl chloride (PVC) using micromachining and drilling in plastic. The inlet nozzle array is chosen as a 4 × 4 array, while the outlets are organized in a 5 × 5 array in such a way that each inlet is surrounded by four outlets. The diameter of both inlets and outlets is set to 500 μm, since larger diameters will not result in more efficient cooling, as shown in Fig. 7. Fig. 12 shows an exploded view of the design of the different parts of the cooler (cover layer, inlet/outlet plenum divider, nozzle plate, support structure, and copper spacer) that will be mounted on the test chip package and printed circuit board (PCB). In order to separate the inlet flow and outlet flow, an inlet/outlet plenum divider is needed, as indicated in Fig. 12. The part has been fabricated using a 500 μm diameter tool for the micromachining and a 500 μm drill to create the inlets and outlets in the nozzle plate, creating a wall thickness of 200 μm for the inlets through the outlet plenum. Fig. 13 shows different fabricated parts of the 4 × 4 array demonstrator of the impingement cooler. It also shows the assembly of the cooler on the thermal test chip and PCB using an O-ring to prevent leakage of the coolant. The presence of the O-ring creates a stand-off of 400 μm between the electronic device and the nozzle plate, which is the cavity where the impingement takes place. After assembly, the cooler has been successfully tested and no leakage was observed.

IV. Thermal Characterization and Benchmarking

Fig. 14 shows the experimental test set-up for the flow or pressure control and for the accurate flow, pressure, and temperature measurements. All the sensors in the set-up are connected

Authorized licensed use limited to: Purdue University. Downloaded on January 16,2023 at 20:04:53 UTC from IEEE Xplore. Restrictions apply.

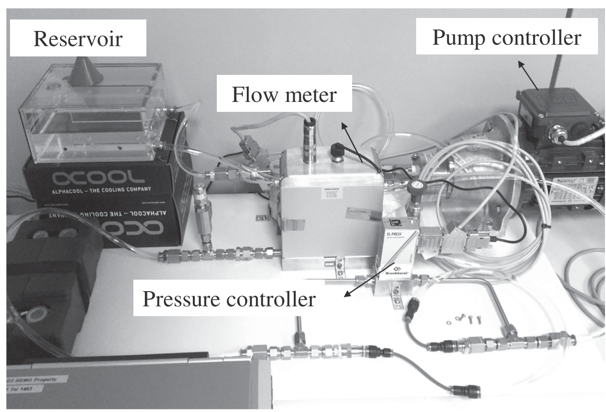

Fig. 14. Schematic of the experimental flow loop.

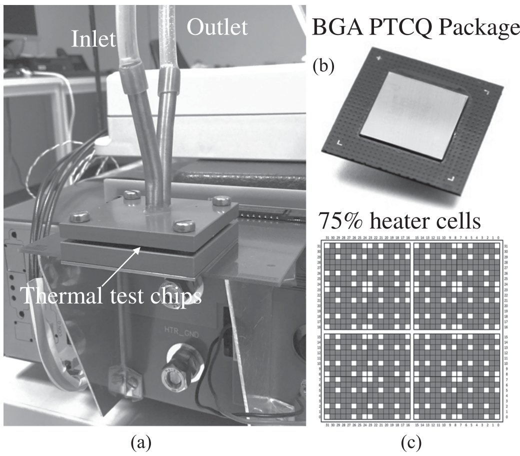

Fig. 15. Multi-jet impingement jet cooler demonstration. (a) Impingement jet cooling setup. (b) and (c) Image of the thermal test chip with heater map and temperature sensor map.

to and controlled by LabView, allowing operation of the flow loop either in a controlled mass flow rate mode or a controlled pressure mode. The accuracy of a mini-Cori flow meter is $\pm 0.2\%$ RD. A differential pressure gauge is used that can withstand a static pressure of 10 bar and measure a pressure drop between 0.2 and 5 bar. The accuracy is $< \pm 0.5\%$ FS. A stainless steel basket filter is used for the pump with a screen of 25 μm. Thermocouples are used to measure the outlet temperature with an accuracy of ± 0.3 °C. The inlet temperature is set as 10 °C. In this study, a dedicated thermal test chip, named PTCQ, is used to study the temperature response of impingement jet cooling. Fig. 15 shows the images of experimental set up and thermal test chip with multi-jet cooler. The programmable test chip with 8×8 mm^2 contains a 32×32 array of temperature sensors for measuring the full chip temperature distribution map. The heaters are constituted by metal meanders resistors in the BEOL that are controlled independently by switches distribution map, resulting in a programmable power map with 832 heater cells with 75% heater uniformity, as shown in Fig. 15(c). The test chip is packaged in a 14×14 mm^2 bare die flip-chip ball grid array package, which allows direct cooling from the backside of the test chip. The 95% confidence interval of the calibrated sensitivity of the temperature sensor on the test chip is –1.55 $\pm$ 0.02 mV/°C for a current of 5 μA in the temperature range between 10 and 75 °C. The measurement uncertainty for the sensor and heater voltage are 1 and 1.6 mV, respectively. The analysis of the propagated measurement uncertainty results in a value of $\pm 1.8\%$ for the reported thermal resistance measurements.

A. Thermal Measurement and Model Validation

The fabricated cooler is characterized for the following conditions: 50 W quasi-uniform chip power, inlet temperature 10 °C, and coolant flow rate ranges from 280 to 600 ml/min. A very low thermal resistance of 0.25 K/W (based on the average chip temperature) is obtained for a flow rate of 600 ml/min with a required pump power of 0.4 W. Moreover, the temperature distribution over the chip is very uniform (see Fig. 16). Compared with a single-jet cooler, shown in Fig. 16(a), on the same chip package, the multi-jet impingement cooler results in a lower thermal resistance and a better temperature uniformity for the same flow rate compared to the single-jet cooler. By increasing the flow rate from 280 to 600 ml/min, the thermal resistance can be reduced by a factor of 1.7. The extracted correlation between the flow rate and the thermal resistance reveals an exponent of –0.66, which agrees well with the typical range –0.6 to –0.8 reported in the literature for submerged impingement cooling [22]. The modeling approach has been validated by comparing the temperature profile in the active region of the chip with the measurement data in the sensors for different flow rates. A very good agreement is obtained between the modeling results and the experimental data. The comparison between the full cooler model and the measurements is shown for the diagonal of the chip temperature in Fig. 16(b), while the comparison of the average chip temperature is presented for the unit cell model, the full cooler model, and the experiments for flow rates from 50 ml/min up to 600 ml/min.

B. Benchmarking With State-of-the-Art Cooling

The cooling performance in terms of thermal resistance and pumping power of the fabricated polymer cooler with a 4×4 array of inlets (0.25 K/W or 0.16 cm^2·K/W for a pumping power of 0.4 W) is compared in Fig. 17 with published data in the literature for impingement coolers fabricated using various materials: Si [10], [11], ceramic [12], metal [5], [7], [13]–[15], and plastic [16], [17] presented in Section I. To assess the tradeoff between the cooling performance and the required pumping power for the liquid coolant, the results are compared in the thermal resistance versus pumping power chart, shown in Fig. 4. Since the literature measurement data of the cooling and hydraulic performance are reported for different chip sizes, the data need to be normalized in order to compare the intrinsic cooling performance of the different coolers. The thermal resistance scales inversely proportional with the chip size (resulting in lower thermal resistance values for large chips), while the pumping power scales proportionally with the area (resulting in high required pumping power for large chips). The proposed metrics for the benchmarking assessment in Fig. 17 are, therefore, the normalized thermal resistance $R_{\text{th}}^* = R_{\text{th}}A$, and the normalized pumping power $W_{\text{p}}* = W_{\text{p}}/A$. The two measurement points of this work (imec-polymer cooler) shown in this figure are based on the fabricated 3-D-shaped polymer cooler

Authorized licensed use limited to: Purdue University. Downloaded on January 16,2023 at 20:04:53 UTC from IEEE Xplore. Restrictions apply.

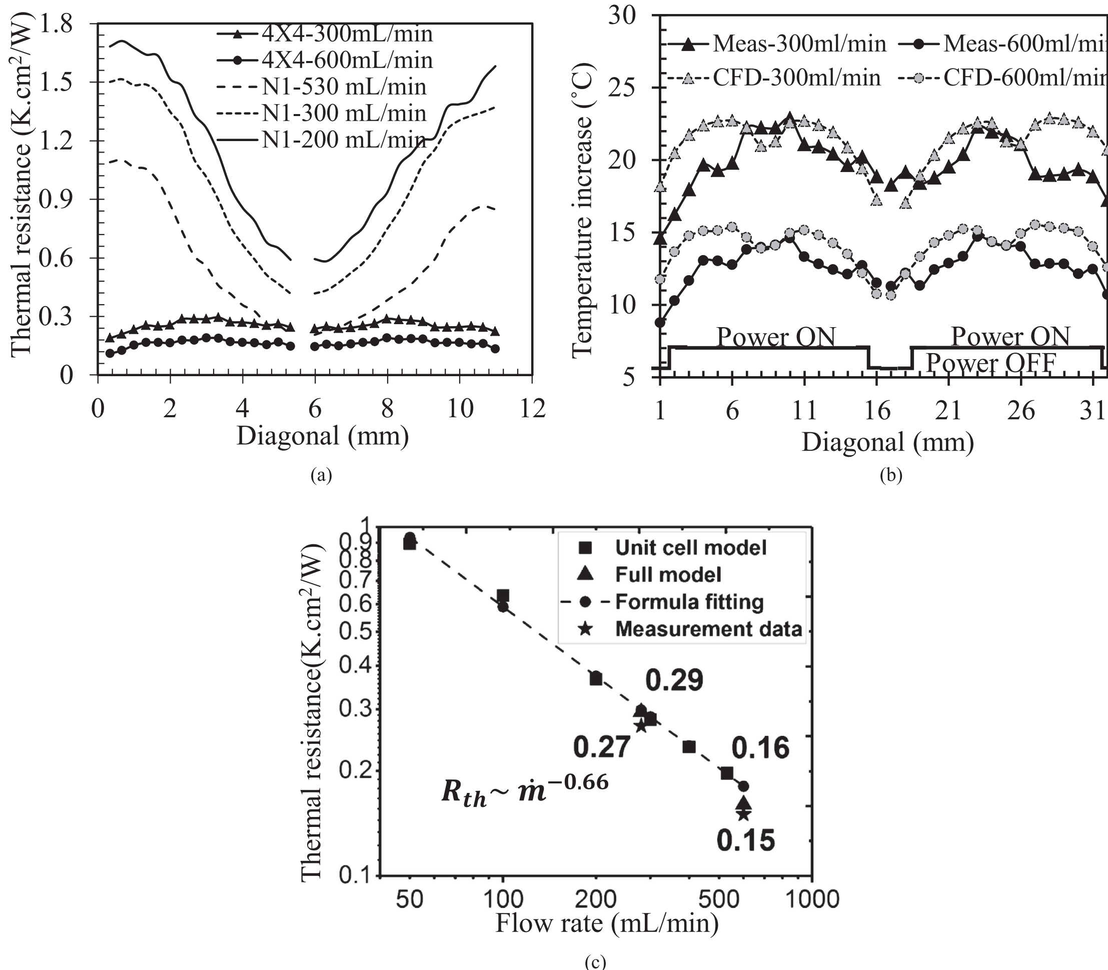

Fig. 16. (a) Comparison of the measured temperature profiles for the cases of the single-jet cooler and the multi-jet 4 × 4 array cooler. (b) Comparison of the chip temperature profile along the chip diagonal between the full cooler CFD simulations and experiments for the 4 × 4 array jet cooler. (c) Average chip temperature comparison for the unit cell and full cooler CFD models and measurement data for different flow rates.

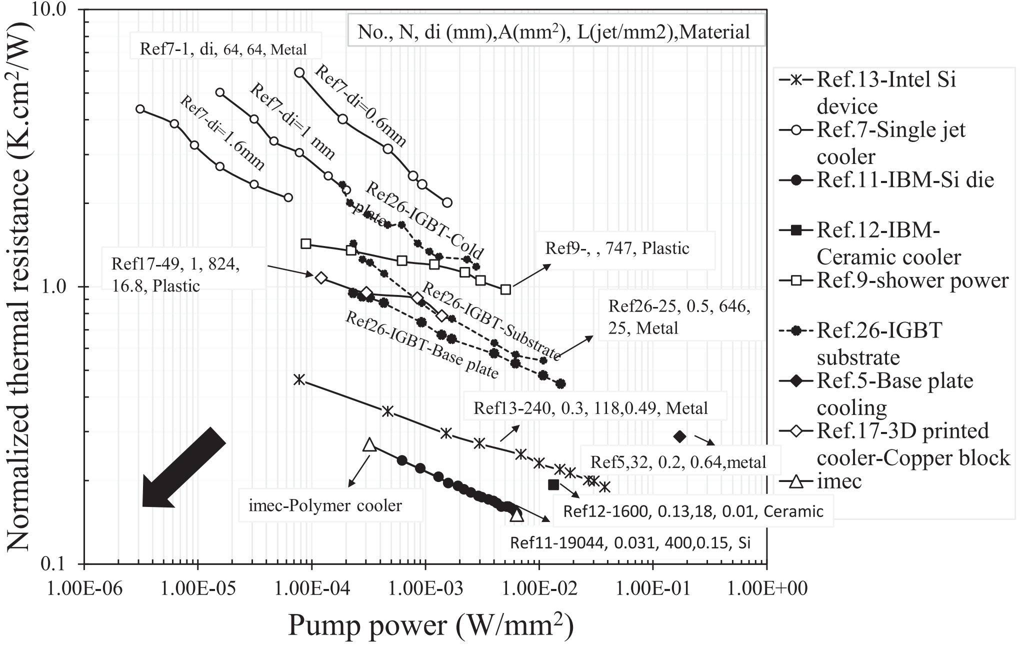

Fig. 17. Thermal performance and pump power comparison with state-of-the-art cooling solutions.

Authorized licensed use limited to: Purdue University. Downloaded on January 16,2023 at 20:04:53 UTC from IEEE Xplore. Restrictions apply.

with a flow rate of 280 and 600 ml/min. From the benchmarking chart in Fig. 17, it can be observed that the presented 3-D-shaped polymer cooler has a very good thermal performance, which is achieved with a relatively low pumping power. The thermal performance of the polymer cooler is very similar to the Si-based cooler [11] with very fine pitch 25 μm diameter nozzles; however, that cooler requires expensive Si fabrication techniques. Comparison with the single-jet cooler [7] applied on a single MOSFET semiconductor device shows that single-jet impingement cooling can be operated at lower pumping power, especially for large nozzle diameters, but that the obtained thermal resistance of single-jet cooling is much higher: the multi-jet cooler outperforms the single-jet cooler by one order of magnitude. The comparison with the results of the cooler for IGBT devices shows the impact of the direct cooling on the semiconductor device: in [26], it is shown that impingement cooling on the base plate is clearly more efficient than cooling on the substrate or using a cold plate. The use of direct liquid multi-jet impinging on the chip backside results in a further improvement of a factor 4 compared to the cooling on the base plate. This benchmarking study clearly shows the potential of the presented multi-jet polymer based cooler and proves that it is not necessary to scale down the nozzle diameters to a few tens of micron, but that very good thermal performance can be obtained with nozzle diameters in the range of several hundred micrometers, which is compatible with low-cost polymer fabrication.

V. Conclusion

Liquid jet impingement cooling is known to be a very efficient cooling technology. State-of-the-art highly efficient multi-jet cooling solutions rely on expensive Si or ceramic fabrication techniques, while cost-efficient cooling solutions have been proposed for less performant single-jet impingement. In this paper, we present the concept, modeling, design, fabrication, experimental characterization, and benchmarking with literature data of a novel multi-jet impingement based liquid cooling solution, fabricated using low-cost polymer fabrication techniques, targeted to directly cool the backside of high-power devices. It is demonstrated that polymer is a valuable alternative material for the fabrication of the impingement cooler instead of expensive Si-based fabrication methods. Unit cell thermal and hydraulic CFD models have been used to study the scaling trends for nozzles dimensions, while full cooler models have been applied to study the interactions between nozzles and the impact of the cooler material. The modeling results show that it is not necessary to scale up the number of unit cells and to shrink the nozzle diameter accordingly to improve the thermal performance for a fixed cavity height, making the required diameters compatible with polymer fabrication methods. Moreover, the simulations indicate that the thermal conductivity of the cooler material has no impact on the thermal performance of the impingement cooler. A 4×4 array jet impingement cooler with 500 μm nozzles has been fabricated using mechanical machining in PVC and has been assembled to a test chip package. The experimental characterization shows a very low thermal resistance of 0.25 K/W (0.16 $\text{cm}^2\cdot$K/W) and good temperature uniformity across the chip surface. The experimental validation shows a good agreement between both the unit cell of the full cooler CFD models and the experimental results. The benchmarking study with literature data for impingement coolers with a large range of inlet diameters shows a very good thermal performance of the fabricated polymer cooler for a low required pumping power. The benchmarking study confirms furthermore that multi-jet cooling is more efficient than single-jet cooling and that direct cooling on the backside of the semiconductor device is more efficient than cooling the substrate or base plate.

References

[1] H. Amano et al., "The 2018 GaN power electronics roadmap," *J. Phys. D, Appl. Phys.*, vol. 51, no. 16, Mar. 2018, Art. no. 163001.

[2] A. S. Bahman and F. Blaabjerg, "Optimization tool for direct water cooling system of high power IGBT modules," in *Proc. Eur. Conf. Power Electron. Appl.*, 2016, pp. 1–10.

[3] S. V. Garimella, T. Persoons, J. A. Weibel, and V. Gektin, "Electronics thermal management in information and communications technologies: Challenges and future directions," *IEEE Trans. Compon., Packag. Manuf. Technol.*, vol. 7, no. 8, pp. 1191–1205, Aug. 2016.

[4] S. Kandlikar, S. Garimella, D. Li, S. Colin, and M. R. King, *Heat Transfer and Fluid Flow in Minichannels and Microchannels*. Oxford, U.K.: Elsevier, 2014, ch. 3.

[5] K. Gould, S. Q. Cai, C. Neft, and S. Member, "Liquid jet impingement cooling of a silicon carbide power conversion module for vehicle applications," *IEEE Trans. Power Electron.*, vol. 30, no. 6, pp. 2975–2984, Jun. 2015.

[6] A. S. Rattner, "General characterization of jet impingement array heat sinks with interspersed fluid extraction ports for uniform high-flux cooling," *J. Heat Transf.*, vol. 139, no. 8, Aug. 2017, Art. no. 082201.

[7] J. Jorg, S. Taraborrelli, G. Sarriegui, R. W. De Doncker, R. Kneer, and W. Rohlfs, "Direct single impinging jet cooling of a mosfet power electronic module," *IEEE Trans. Power Electron.*, vol. 33, no. 5, pp. 4224–4237, May 2018.

[8] A. Bhunia and C. L. Chen, "On the scalability of liquid microjet array impingement cooling for large area systems," *J. Heat Transf.*, vol. 133, no. 6, Jan. 2011, Art. no. 064501.

[9] K. Olesen, R. Bredtmann, and R. Eisele, "'Shower power' new cooling concept for automotive applications," in *Proc. Automot. Power Electron.*, Jun. 2006, pp. 1–9.

[10] E. N. Wang et al., "Micromachined jets for liquid impingement cooling for VLSI chips," *J. Microeletromech. Syst.*, vol. 13, no. 5, pp. 833–842, Oct. 2004.

[11] T. Brunschwiler et al., "Direct liquid jet-impingement cooling with micronsized nozzle array and distributed return architecture," in *Proc. IEEE Therm. Thermomech. Phenom. Electron. Syst.*, 2006, pp. 196–203.

[12] G. Natarajan and R. J. Bezama, "Microjet cooler with distributed returns," *Heat Transf. Eng.*, vol. 28, nos. 8–9, pp. 779–787, Jul. 2010.

[13] T. Acikalin and C. Schroeder, "Direct liquid cooling of bare die packages using a microchannel cold plate," in *Proc. IEEE Therm. Thermomech. Phenom. Electron. Syst.*, 2014, pp. 673–679.

[14] S. Liu, T. Lin, X. Luo, M. Chen, and X. Jiang, "A microjet array cooling system for thermal management of active radars and high-brightness LEDs," in *Proc. IEEE Electron. Compon. Technol. Conf.*, 2006, pp. 1634–1638.

[15] M. R. Overholt, A. McCandless, K. W. Kelly, C. J. Becnel, and S. Motakef, "Micro-jet arrays for cooling of electronic equipment," in *Proc. ASME 3rd Int. Conf. Microchannels Minichannels*, 2005, pp. 249–252.

[16] M. Baumann, J. Lutz, and W. Wondrak, "Liquid cooling methods for power electronics in an automotive environment," in *Proc. 2011 14th Eur. Conf. Power Electron. Appl.*, 2011, pp. 1–8.

[17] B. P. Whelan, R. Kempers, and A. J. Robinson, "A liquid-based system for CPU cooling implementing a jet array impingement waterblock and a tube array remote heat exchanger," *Appl. Therm. Eng.*, vol. 39, pp. 86–94, Jun. 2012.

[18] S. Ndao, H. J. Lee, Y. Peles, and M. K. Jensen, "Heat transfer enhancement from micro pin fins subjected to an impinging jet," *Int. J. Heat Mass Transf.*, vol. 55, nos. 1–3, pp. 413–421, Jan. 2012.

Authorized licensed use limited to: Purdue University. Downloaded on January 16,2023 at 20:04:53 UTC from IEEE Xplore. Restrictions apply.

[19] Y. Han, B. L. Lau, G. Tang, and X. Zhang, "Thermal management of hotspots using diamond heat spreader on Si microcooler for GaN devices," *IEEE Trans. Compon., Packag. Manuf. Technol.*, vol. 5, no. 12, pp. 1740–1746, Dec. 2015.

[20] A. J. Robinson *et al.*, "A new hybrid heat sink with impinging micro-jet arrays and microchannels fabricated using high volume additive manufacturing," in *Proc. IEEE Annu. IEEE Semicond. Therm. Meas. Manage. Symp.*, 2017, pp. 179–186.

[21] H. Oprins, V. Cherman, G. Van der Plas, J. De Vos, and E. Beyne, "Experimental characterization of the vertical and lateral heat transfer in three-dimensional stacked die packages," *J. Electron. Packag.*, vol. 138, no. 1, Mar. 2016, Art. no. 10902.

[22] N. Zuckerman and N. Lior, "Jet impingement heat transfer: Physics, correlations, and numerical modeling," *Adv. Heat Transf.*, vol. 39, pp. 565–631, 2006.

[23] J. Jorg *et al.*, "Hot spot removal in power electronics by means of direct liquid jet cooling," in *Proc. IEEE Therm. Thermomech. Phenom. Electron. Syst.*, 2017, pp. 471–481.

[24] R. Skuriat, "Direct jet impingement cooling of power electronics," Ph.D. thesis, Univ. Nottingham, Nottingham, U.K., 2012.

[25] Y. Han, B. L. Lau, G. Tang, X. Zhang, and D. M. W. Rhee, "Si-based hybrid microcooler with multiple drainage microtrenches for high heat flux cooling," *IEEE Trans. Compon., Packag. Manuf. Technol.*, vol. 7, no. 1, pp. 50–57, Jan. 2017.

[26] R. Skuriat and C. M. Johnson, "Thermal performance of baseplate and direct substrate cooled power modules," in *Proc. 4th IET Int. Conf. Power Electron. Mach. Drives*, 2008, pp. 548–552.

[27] E. A. Browne, G. J. Michna, M. K. Jensen, and Y. Peles, "Microjet array single-phase and flow boiling heat transfer with R134a," *Int. J. Heat Mass Transf.*, vol. 53, nos. 23–24, pp. 5027–5034, Nov. 2010.

[28] E. G. Colgan *et al.*, "A practical implementation of silicon microchannel coolers for high power chips," *IEEE Trans. Compon., Packag. Technol.*, vol. 30, no. 2, pp. 218–225, Jun. 2007.

[29] C. S. Sharma, G. Schlottig, T. Brunschwiler, M. K. Tiwari, B. Michel, and D. Poulikakos, "A novel method of energy efficient hotspot-targeted embedded liquid cooling for electronics: An experimental study," *Int. J. Heat Mass Transf.*, vol. 88, pp. 684–694, Sep. 2015.

[30] M. K. Sung and I. Mudawar, "Single-phase hybrid micro-channel/micro-jet impingement cooling," *Int. J. Heat Mass Transf.*, vol. 51, nos. 17–18, pp. 4342–4352, Aug. 2008.

Tiwei Wei (S'18) received the M.Sc. degree in electronics engineering from Chongqing University of Posts and Telecommunications, Chongqing, China, and the joint master program with Tsinghua University, Beijing, China, in 2012. He is a Ph.D. Researcher with imec, Leuven, Belgium. He joined imec in 2015, starting the Ph.D. research by developing thermal cooling solutions for high-performance systems. Before joining imec, from 2011 until 2015, he worked as a Researcher Staff with Tsinghua University and Hong Kong University of Science and Technology, where he was responsible for the test vehicles design, process development, and experimental characterization in 3-D system integration technologies related to 3-D/2.5-D integration, through silicon via, and through glass via. He authored more than 11 publications in IEDM, ECTC, EPTC, etc. Moreover, he holds nine Chinese national patents and one U.S. patent in the area of advanced packaging.

Mr. Wei was a recipient of an Outstanding Paper Award in ICEPT 2013.

Herman Oprins received the M.Sc. and Ph.D. degrees in mechanical engineering from the Katholieke Universiteit (KU) Leuven, Leuven, Belgium, in 2003, and 2008 respectively.

He joined imec, Leuven, Belgium, in 2003, working toward the Ph.D. degree with KU Leuven and working on modeling and experimental projects on thermal management of electronic packages. Since 2009, he has been working as a Senior Research Engineer with imec, where he is involved in the thermal experimental characterization, thermal modeling, and management of 3-D ICs, electronic packages, GaN transistors, photovoltaic modules, and microfluidics.

Vladimir Cherman received the M.S. and Ph.D. degrees in electronic engineering from Saint Petersburg Electrotechnical University, St. Petersurg, Russia, in 1994 and 1999, respectively.

From 1997 to 2000, he was an Electronics Engineer with Morion, Inc., St. Petersurg. From 2000 to 2007, he was with the Ceramics Laboratory, Swiss Federal Institute of Technology-Lausanne, Lausanne, Switzerland, where he researched microwave properties of ferroelectric materials. Since 2007, he has been a Researcher with imec, Leuven, Belgium, where he is involved in reliability studies of microelectromechanical systems devices and electronic packages.

Jun Qian received the Ph.D. degree in mechanical engineering from the Nanjing University of Aeronautics and Astronautics, Nanjing, China, in 1996.

His research interests include micro- and precision machining processes, design of precision mechanism, and precision metrology. In 2000, he joined the Mechanical Engineering Department, Katholieke Universiteit Leuven, Leuven, Belgium, where he has been a Staff Research Manager, since 2009. He is currently also an affiliated Flanders Make Corelab Manager, focusing on sensing and monitoring for manufacturing processes.

Ingrid De Wolf received the Ph.D. degree in physics from the Katholieke Universiteit (KU) Leuven, Leuven, Belgium in 1989.

In 1989, she joined imec, Leuven, Belgium, where she worked in the field of microelectronics reliability. From 1999 to 2014, she headed the group REMO, focused on reliability, test, and modeling. She authored or coauthored several book chapters and more than 350 publications. She is the Chief Scientist in imec and a Professor with the Department of Materials Engineering, KU Leuven.

Eric Beyne (M'83) received the master's degree in electrical engineering and the Ph.D. degree in applied sciences from the Katholieke Universiteit Leuven, Leuven, Belgium, in 1983 and 1990, respectively.

Since 1986, he has been with imec, Leuven, where he has been involved in advanced packaging and interconnect technologies. He is currently a fellow with imec, where he is the Program Director of the 3-D System Integration Program.

Martine Baelmans received the Ph.D. degree in engineering from the Katholieke Universiteit (KU) Leuven, Leuven, Belgium, in 1993.

She is a Professor with the Department of Mechanical Engineering at the KU Leuven in Belgium, where she leads the group on thermal-fluid engineering since 1996. She has authored or coauthored more than 200 papers in applications on fluid mechanics and heat transfer. Research topics are presently focusing on automated optimization in thermal design. Starting from dedicated component and system models, parameters, shapes and topologies are improved. Applications range from liquid and two-phase cooling over thermal management in power electronics, power transformers and energy systems.

Authorized licensed use limited to: Purdue University. Downloaded on January 16,2023 at 20:04:53 UTC from IEEE Xplore. Restrictions apply.